Drug Development Research

WILEY

DRUG DEVELOPMENT RESEARCH

RESEARCH ARTICLE OPEN ACCESS

Hexahydroquinoline Featuring Amide Functionality: A Promising Scaffold With Calcium Channel Blocking Activity

Ebru Koçak Aslan[1] | Kevin Lam[2] | Sun Huang[3] | Göknil Pelin Coşkun[4] | Ayşe Karagüzel[1,5] | Katrin Denzinger[2] | Kaan Birgül[6] | Mert Ülgen[4] | Jordan W. Nafie[7] | Onur Şahin[8] | Daniel W. Armstrong[9] | Gerald W. Zamponi[3] | Gerhard Wolber[2] | Miyase Gözde Gündüz[1]

[1]Department of Pharmaceutical Chemistry, Faculty of Pharmacy, Hacettepe University, Ankara, Turkey | [2]Molecular Design Group, Department of Pharmaceutical and Medicinal Chemistry, Institute of Pharmacy, Freie Universität Berlin, Berlin, Germany | [3]Department of Clinical Neurosciences, Hotchkiss Brain Institute and Alberta Children's Hospital Research Institute, University of Calgary, Calgary, Alberta, Canada | [4]Department of Pharmaceutical Chemistry, Faculty of Pharmacy, Acıbadem University, Istanbul, Turkey | [5]Department of Pharmaceutical Chemistry, Faculty of Pharmacy, Başkent University, Bağlıca, Turkey | [6]Department of Pharmaceutical Chemistry, Faculty of Pharmacy, Bahçeşehir University, Istanbul, Turkey | [7]BioTools, Inc., West Palm Beach, Florida, USA | [8]Department of Occupat Health & Safety, Faculty of Health Sciences, Sinop University, Sinop, Turkey | [9]Department of Chemistry & Biochemistry, University of Texas at Arlington, Arlington, Texas, USA

Correspondence: Miyase Gözde Gündüz (miyaseg@hacettepe.edu.tr; miyasegunduz@yahoo.com)

Received: 23 June 2025 | **Revised:** 25 January 2026 | **Accepted:** 27 February 2026

Funding: Hacettepe University Scientific Research Projects Coordination Unit, Grant/Award Number: THD-2024-21388; Natural Sciences and Engineering Research Council of Canada

Keywords: dihydropyridine | enantioseparation | Hantzsch synthesis | metabolic stability | molecular modeling | patch clamp

ABSTRACT

Hexahydroquinoline (HHQ) is a widely recognized scaffold that has garnered considerable attention owing to its diverse pharmacological properties. The structure of HHQ includes a 1,4-dihydropyridine (DHP) ring, which serves as the pharmacophore for the predominant class of drugs known as calcium channel blockers. DHPs are frequently utilized in the management of cardiovascular diseases and also show potential for pain management. Since all DHPs on the market possess ester functionality, we aimed to employ bioisosteric replacement to observe if their amide-containing counterparts would still block calcium channels. Therefore, we synthesized new HHQs with ester or amide functionality (**EM1**-**EM15**) and investigated their effects on L-($Ca_v1.2$) and T-($Ca_v3.2$)-type calcium channels using the whole-cell patch clamp technique. Although the amide derivatives were somewhat less effective than their ester counterparts, they still blocked calcium channels to a significant degree. Retesting **EM4** enantiomers on two types of calcium channels demonstrated that the (*R*)-isomer was more responsible for the blocking activity in both cases. Molecular docking and molecular dynamics simulations demonstrated that **(*R*)-EM4** and **(*R*)-EM6** adopt binding modes in $Ca_v1.2$ similar to amlodipine, while showing favorable stability. Docking studies in $Ca_v3.2$ suggested that EM compounds bind within the III-IV fenestration, a reported non-selective DHP binding site. Furthermore, amide derivatives were found to be more metabolically stable based on the in vitro experiments conducted on rat microsomes. Overall, our study reveals HHQ with an amide group as a promising new scaffold for developing future calcium channel blockers for treating cardiovascular and pain conditions.

1 | Introduction

Voltage-gated calcium channels serve as the principal conductors of the entry of calcium ions (Ca^{2+}) into a range of electrically excitable cells within the body (Catterall 2023). Elevated intracellular calcium levels have been associated with a broad spectrum of physiological functions including neurotransmitter release, hormone secretion, and muscle contraction (Bkaily and Jacques 2023). Hence, compromised calcium signaling can lead to various pathological conditions, such as hypertension and neurological disorders (Glaser et al. 2019).

Selective inhibition of calcium currents in cardiac and smooth muscle through the administration of calcium blockers, mainly 1,4-dihydropyridines (DHPs), represents a widely adopted therapeutic approach in the treatment of cardiovascular disorders (KE; Jones et al. 2024). The $Ca_v1.2$ isoform of voltage-gated calcium channels, which exhibits unique electrophysiological and pharmacological properties among other subtypes, is the principal target of DHP drugs such as nifedipine, amlodipine, and so on that are commonly prescribed for the management of hypertension and angina pectoris (Hofmann et al. 2014; Bain 2019).

While DHPs are well-established for their ability to inhibit L-type calcium channels, some DHP-based molecules have also demonstrated the capacity to modulate the T-type calcium channel family (Bladen et al. 2015; Akman et al. 2022; Aygün Cevher et al. 2019). Among three distinct isoforms ($Ca_v3.1$-$Ca_v3.3$) with specific physiological roles, the $Ca_v3.2$ subtype has been found to play a key part in the regulation of pain signaling, and its increased activity has been linked to a variety of chronic pain conditions arising from nerve injury, diabetes, and chemotherapeutic treatment (Weiss and Zamponi 2019; Harding and Zamponi 2022; Weiss and Zamponi 2023). Consequently, the $Ca_v3.2$ channel emerges as a promising target for the development of novel analgesic therapeutics (Cai et al. 2021).

Due to their significant position among calcium channel blockers, modification of the DHP framework has been the focus of many research studies (Saini et al. 2023). Prior studies have primarily explored modifying the alkyl substituents on the ester groups of DHPs, including the commercially available molecules within this class of compounds (Bandyopadhyay et al. 2017). Furthermore, incorporating the DHP scaffold into a fused ring system such as hexahydroquinoline (HHQ) has also resulted in the identification of novel and potent inhibitors of various calcium channel subtypes (Schaller et al. 2018; Bladen et al. 2014).

When the chemical structures of commercial DHPs, according to the Anatomical Therapeutic Chemical Classification System (ATC Code: C08CA), are analyzed, it can be seen that despite extensive chemical modifications in its alkyl side chain, ester moiety has never been replaced with amide functionality (Figure 1) (Nahler 2009).

Bioisosteric substitution is a widely applied strategy in the rational modification of lead compounds, as this approach can result in enhanced potency, optimized pharmacokinetic properties and decreased toxicity (Meanwell 2023). As the amide functionality is a key structural feature in the composition of numerous pharmacologically active compounds, we aimed to swap the ester moiety of DHP-based calcium channel blockers with amide group (Kumari et al. 2020). In this way, we aimed to obtain a new scaffold, HHQ with amide functionality, for calcium channel inhibition by applying the principle of bioisosterism. Additionally, we synthesized ester derivatives as the chemically-similar analogues of these amides (Figure 2).

After confirming the proposed chemical structures, the molecules were tested for their inhibition capacity against $Ca_v1.2$ and $Ca_v3.2$ channels. Furthermore, the metabolic stability of the compounds were investigated and the physiological data obtained were supported by molecular modeling techniques.

2 | Material and Methods

2.1 | Chemistry

Synthesis of the target compounds was carried out by a modified Hantzsch reaction. An equimolar amount of 5,5-dimethyl-1,3-cyclohexanedione (dimedone), benzyl acetoacetate/

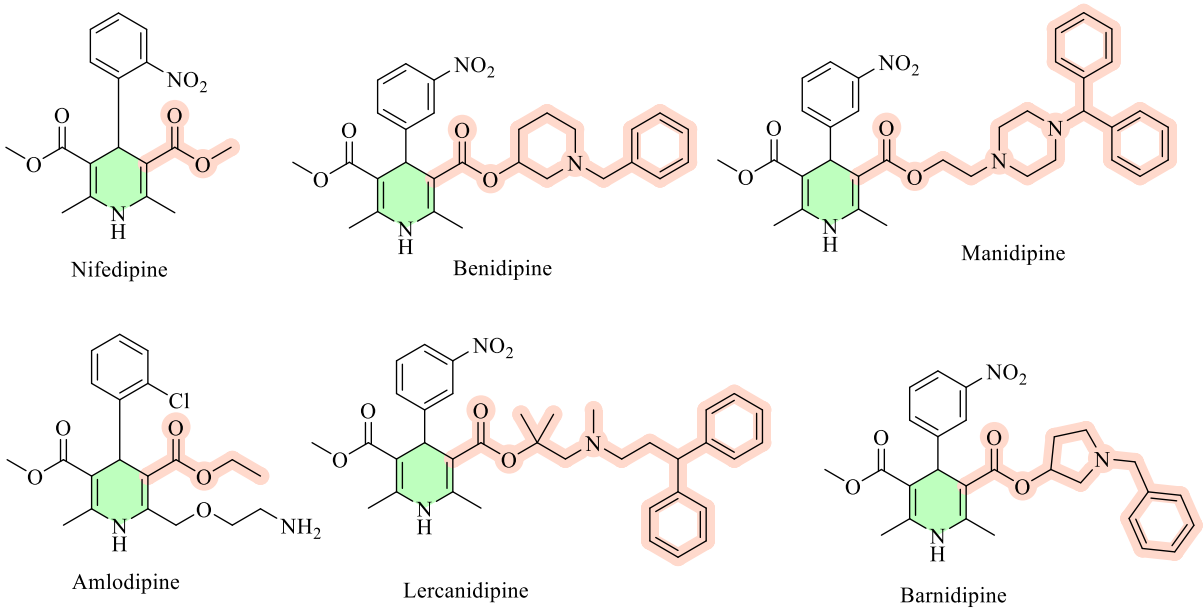

FIGURE 1 | Examples of certain commercial DHP-type calcium channel blockers with varying ester groups.

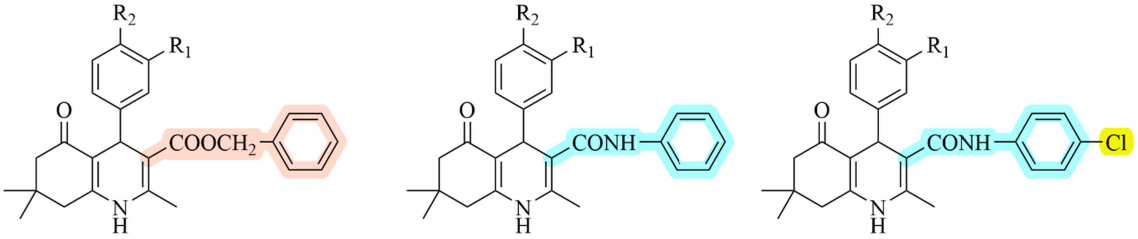

FIGURE 2 | General chemical structures of the target HHQs (**EM1**-**EM15**) with ester or amide functionality.

acetoacetanilide/4-chloroacetoacetanilide, appropriate aldehyde, and excess ammonium acetate were refluxed in absolute ethanol (20 mL) for 8–10 h. After completion, the reaction mixture was cooled, and obtained product was filtered. All solid products were crystallized from ethanol except for **EM2**, **EM3,** and **EM5** that were purified by crystallization from ethanol:water (9:1).

2.2 | X-Ray Diffraction Analysis

Suitable crystal of **EM14** was selected for data collection which was performed on a Bruker diffractometer equipped with a graphite-monochromatic Mo-K_α radiation at 296 K. We used these procedures for our analysis: solved by direct methods; SHELXS-2013 (Sheldrick 2008); refined by full-matrix least-squares methods; SHELXL-2013 (Sheldrick 2015); data collection: Bruker APEX3 (Bruker AXS Inc. 2012); molecular graphics: MERCURY (MacRae et al. 2020); solution: WinGX (Farrugia 2012). Crystallographic data for the structural analysis has been deposited with the Cambridge Crystallographic Data Centre, CCDC No. 2344906.

2.3 | Whole-Cell Patch Clamp Assay

Calcium channel blocking capacity of the compounds was determined against $Ca_v1.2$ and $Ca_v3.2$ by applying whole-cell patch clamp assay as reported previously (Akman et al. 2022). Data analysis was performed using GraphPad Prism 5 (GraphPad Software, La Jolla, CA). All data results are presented as mean values ± standard errors of the mean. n values given in the figures reflect numbers of cells tested.

2.4 | Enantioseparation of EM4 and Absolute Configuration Determination

EM4 was dissolved in acetonitrile (Fisher Scientific, Waltham, MA, USA) at a concentration of ~1 mg/mL. (*S*,*S*)-WhelkoShell column was obtained from AZYP LLC (Arlington, TX, USA) in the dimension of 150 mm x 4.6 mm (i.d.), with 2.7 μm superficially porous particles (SPP). The analytical and preparative separations were done on an Agilent 1220 Infinity II LC System (Product No. G4290B) supported by the OpenLAB Software Version 2.2. ~8 mg of **EM4** (P1 or P2) was dissolved in 135 μL $CDCl_3$ to collect IR and VCD spectra (Armstrong et al. 2021). The *R* enantiomer of **EM4** was constructed using ComputeVOA software, resulting in 28 conformers within a 7 kcal/mol energy window. Initial DFT calculations were performed at the 6-31 G (d) level with CPCM (Chloroform). The 22 lowest energy conformers were further optimized at the cc-pVTZ level. These conformers were Boltzmann averaged, frequencies scaled by 0.984, and plotted as Lorentzian bands for comparison to experiment (Freedman et al. 2003).

2.5 | Molecular Modeling Studies

2.5.1 | *Molecular Docking*

The Cryo-EM structure of human $Ca_v1.2$ in complex with amlodipine (PDB: 8WE8) (Gao et al. 2023) and human $Ca_v3.2$ (PDB 9AYH) (Huang et al. 2024) was used to create the template for molecular docking. Molecular docking studies were then performed for **EM4** and **EM6** in the DHP cavity of $Ca_v1.2$ using GOLD (v2020; Genetic Optimization for Ligand Docking, The Cambridge Crystallographic Data Center, UK) (G. Jones et al. 1997). Atoms within a 6 Å radius around amlodipine were defined as part of the binding site. Twenty binding hypotheses for each compound were generated in the DHP binding site, minimized in the MMFF94 force field and then visually inspected (Halgren 1996). Binding modes that form a hydrogen bond with Ser1132 were preferred over others, resulting in one final binding mode for each compound.

For $Ca_v3.2$, molecular docking studies were initially performed for all EM compounds in the binding site of the co-resolved phospholipid within the III-IV fenestration, a radius of 10 Å around the phospholipid. Then, only ***(R)*-EM4** and ***(R)*-EM6** were considered and twenty binding mode hypotheses were generated. A distance constraint was applied between the backbone carbonyl oxygen of Ser1501 and the *N*-1 hydrogen of the HHQ moiety. 3D pharmacophores were generated in Ligandscout (v4.4.3; InteLigand, Vienna, Austria) (Wolber and Langer 2005; Wolber et al. 2006) to filter out poses which did not fulfill a hydrogen bond between the *N*-1 hydrogen and either the backbone carbonyl oxygen or the hydroxyl oxygen of Ser1501.

2.5.2 | *Molecular Dynamics Simulations*

The stability and dynamic interaction patterns of the binding modes of ***(R)*-EM4** and ***(R)*-EM6** were further analyzed using MD simulations. The protein-ligand complexes of ***(R)*-EM4** and ***(R)*-EM6** in $Ca_v1.2$, obtained from the molecular docking studies, were first prepared in Maestro (v13.1.137; Schroedinger LLC, New York City, NY, USA). The prepared systems were then simulated five times using Desmond (v2022.01; Schroedinger LLC, New York City, NY, USA) for 50 ns on graphic processing units on the Freie Universität Cluster. Simulations were performed utilizing the OPLS2005 force field (Jorgensen et al. 1996). In the final step, dynophores were generated for ***(R)*-EM4** and ***(R)*-EM6**. Dynophores is an in-house application that tracks possible protein-ligand interactions on each frame of

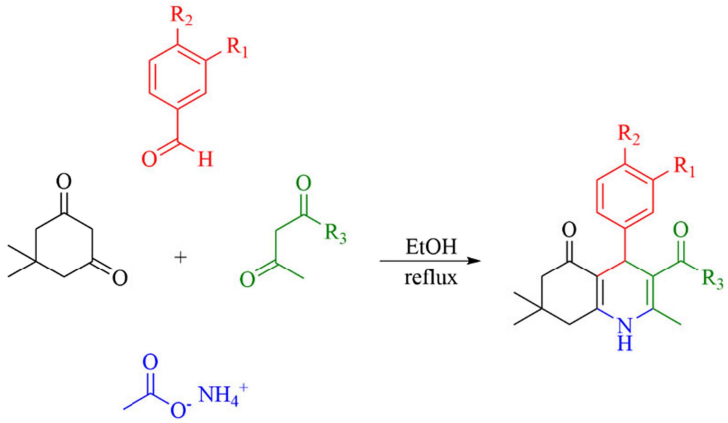

Compound	R_1	R_2	R_3
EM1	NO_2	Cl	-O-CH_2-C_6H_5
EM2	NO_2	Cl	-NH-C_6H_5
EM3	NO_2	Cl	-NH-(*p*-Cl-C_6H_4)
EM4	F	Cl	-O-CH_2-C_6H_5
EM5	F	Cl	-NH-C_6H_5
EM6	F	Cl	-NH-(*p*-Cl-C_6H_4)
EM7	CF_3	Cl	-O-CH_2-C_6H_5
EM8	CF_3	Cl	-NH-C_6H_5
EM9	CF_3	Cl	-NH-(*p*-Cl-C_6H_4)
EM10	OCH_3	OCH_3	-O-CH_2-C_6H_5
EM11	OCH_3	OCH_3	-NH-C_6H_5
EM12	OCH_3	OCH_3	-NH-(*p*-Cl-C_6H_4)
EM13	-O-CH_2-O-		-O-CH_2-C_6H_5
EM14	-O-CH_2-O-		-NH-C_6H_5
EM15	-O-CH_2-O-		-NH-(*p*-Cl-C_6H_4)

FIGURE 3 | Chemical structures and synthesis of the target HHQs investigated in this study.

an MD simulation and summarizes them as interaction clouds (Schaller et al. 2020).

2.6 | Metabolic Stability Determination

Metabolic stability determination of **EM1**-**EM3** was performed on Wistar albino rat liver microsomes according to the previously reported procedure (Pelin COŞKUN et al. 2023). All animal research procedures were followed in accordance with the standards set forth in the eighth edition of Guide for the Care and Use of Laboratory Animals (published by the National Academy of Sciences, The National Academies Press, Washington, D.C.).

3 | Results and Discussion

3.1 | Chemistry

In this study, we synthesized fifteen HHQ derivatives (**EM1**-**EM15)** bearing ester or amide functionality according to a modified Hantzsch reaction. The target molecules were obtained by refluxing equimolar amounts of dimedone, aldehyde derivative, and appropriate dicarbonyl compound (benzyl acetoacetate/acetoacetanilide/4'-chloroacetoacetanilide) in absolute ethanol in the presence of excess ammonium acetate as shown in Figure 3.

The chemical structures of **EM1**-**EM15** were confirmed by a combination of spectroscopic techniques, including ^{1}H NMR, ^{13}C NMR, X-ray analysis, and HRMS. In the ^{1}H NMR spectra, the resonances of the H-4 and N-H protons on the HHQ ring were identified as singlets, appearing at chemical shifts of 4.80–5.04 ppm and 9.06–9.77 ppm, respectively. The presence of a chiral center at C-4 of the HHQ ring results in non-equivalent methylene protons in the benzyl group of ester-carrying derivatives. Consequently, the methylene groups appeared as an AB spin system, with *J* coupling constants of approximately 12.4 Hz. Additionally, singlet signals derived from the N-H proton of the amide functionality observed between 8.67 and 8.93 ppm confirmed the proposed structures of the amide-bearing HHQs. In ^{13}C NMR spectra, carbonyl signals belonging to ester/amide and ketone groups were observed at around 165 and 195 ppm, respectively. In the HRMS analysis, the mass measurements aligned consistently with the calculated molecular weight values.

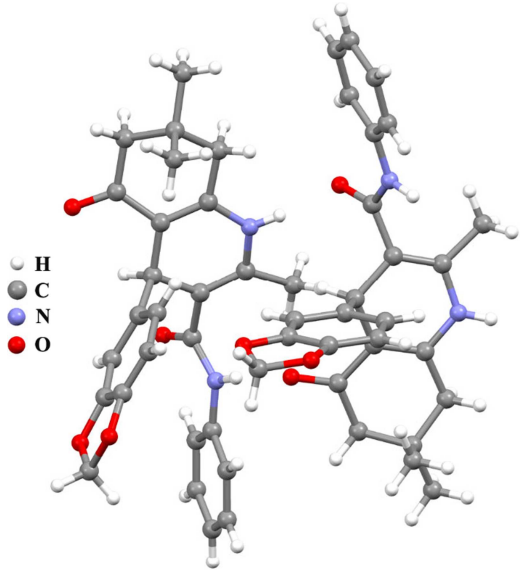

FIGURE 4 | The molecular structure of **EM14**.

Furthermore, isotope peaks were detected for the compounds that carry chlorine. The ^{1}H NMR, ^{13}C NMR, and HRMS data for the target HHQs are provided as supporting material.

3.2 | Crystal Structure of EM14

The proposed chemical structure of **EM14** was also confirmed by single crystal X-ray analysis. The molecular structure of **EM14** with the atomic labeling is shown in Figure 4. The asymmetric unit contains two symmetry independent molecules with no significant difference in their structures.

The C7═O1 [1.236(2) Å], C17═O2 [1.239(2) Å], C33═O5 [1.236(2) Å] and C43═O6 [1.240(3) Å] bond distances are typical double bond character (Table 1).

The C═C double bond distances range from 1.335(3) to 1.363(3) Å, respectively. The torsion angle of C6-N1-C7-C8 is 174.0(2)°, while the torsion angle of C32-N3-C33-C34 is −175.7(2)°. The dihedral angle between the dihydropyridine and benzodioxole rings are 83.15(6)° and 88.84(6)°, while the dihedral angle between the dihydropyridine and phenyl rings are 78.61(6)° and

80.62(7)°. Each cyclohexene ring adopts a half-chair conformation. The puckering parameters (q_2, q_3, Q_T, θ and φ) are 0.3896 Å, -0.2380 Å, 0.4565°, 121.41° and 55.16° for C10-C11-C17-C16-C15-C14 ring and 0.4014 Å, 0.2500 Å, 0.4729°, 58.09° and 237.87° for C36-C37-C43-C42-C41-C40 ring. The molecules of **EM14** are connected by N-H···O hydrogen bonds (Table 2).

The combination of N-H···O hydrogen bonds produces edge-fused $R_2^2(14)$ rings which is running parallel to the [010] direction (Figure 5).

TABLE 1 | Selected bond distances and angles for **EM14** (Å, º).

C7-O1	1.236 (2)	C17-O2	1.239 (2)
C33-O5	1.236 (2)	C43-O6	1.240 (3)
C8-C9	1.338 (3)	C10-C11	1.363 (3)
C34-C35	1.335 (3)	C36-C37	1.360 (3)
C6-N1-C7-C8	174.0 (2)	C32-N3-C33-C34	−175.7 (2)

TABLE 2 | Hydrogen-bond parameters for **EM14** (Å, °).

D-H· · ·A	D-H	H···A	D···A	D-H···A
C14—H14B···O5	0.97	2.57	3.328 (3)	135
N1—H1A···O6	0.86	2.11	2.962 (2)	172
N2—H2A···O5	0.86	2.04	2.871 (2)	163
N3—H3A···O2^{i}	0.86	2.08	2.939 (2)	174
N4—H4A···O1^{i}	0.86	2.14	2.964 (2)	162

Note: Symmetry code: (i) x, y − 1, z.

3.3 | Determination of $Ca_v1.2$ and $Ca_v3.2$ Inhibition

We determined the calcium channel inhibition capacity of the synthesized compounds (**EM1**-**EM15**) on both $Ca_v1.2$ and $Ca_v3.2$ by employing a whole cell patch-clamp assay. Nifedipine as one of the most popular member of commercial DHPs was also tested as positive control (Akman et al. 2022). The data were presented as the percent inhibition of the calcium current observed after applying each **EM** compound and nifedipine at 10 μM concentrations (Figure 6). When the obtained data were analyzed, it was observed that, as expected, nifedipine inhibited the L-type calcium current almost completely while it failed to effectively block T-type calcium channel like many of the DHP-based antihypertensives on the market. On the other hand, eight of our compounds **(EM1**-**EM4**, **EM6**-**EM9**) produced more than 50% block of $Ca_v1.2$ whereas eleven derivatives (**EM1**-**EM4**, **EM6**-**EM10**, **EM13**, and **EM15)** inhibited $Ca_v3.2$ calcium currents by at least 50%. Additionally, not only were more compounds effective inhibitors of $Ca_v3.2$ compared to $Ca_v1.2$, but the compounds generally mediated stronger inhibition of $Ca_v3.2$ compared to $Ca_v1.2$. Within this series, **EM13** and **EM15** stood out in terms of their high selective blocking activity against $Ca_v3.2$ over $Ca_v1.2$.

Subsequent analyses were performed to obtain the dose-response curves of **EM4** and **EM6**, identified as effective inhibitors of $Ca_v1.2$ and $Ca_v3.2$ with ester and amide groups, respectively. Figure 7 illustrates the dose–response curves for the inhibition of $Ca_v1.2$ and $Ca_v3.2$ by **EM4** and **EM6**, along with representative current traces recorded in the absence and presence of 1 μM of the test compound. Additionally, IC_{50} values were calculated from curve fitting of the dose-response data. **EM4** and **EM6**

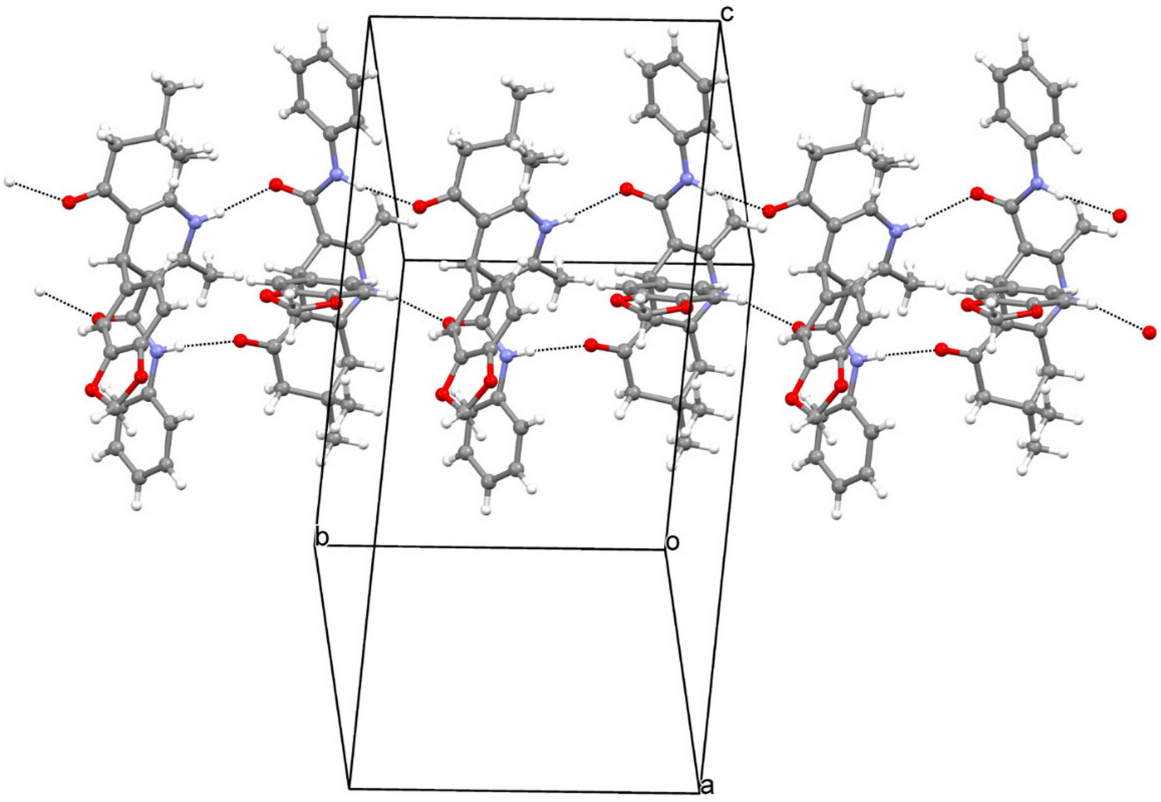

FIGURE 5 | The 1D supramolecular network in **EM14**.

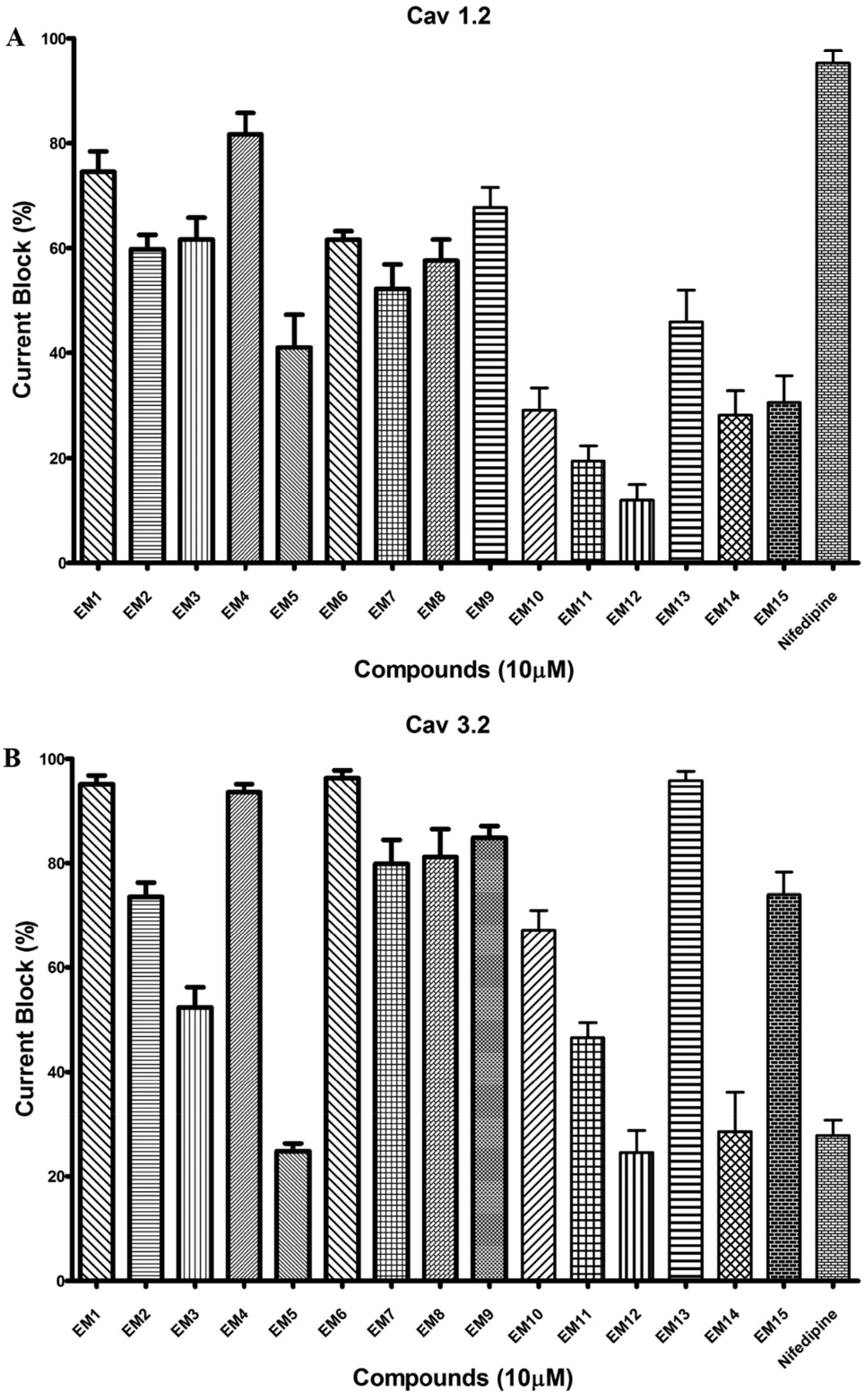

FIGURE 6 | Block of rat $Ca_v1.2$ (A) and human $Ca_v3.2$ (B) by application of 10 μM **EM1**-**EM15** and nifedipine ($n = 3$). Error bars reflect standard errors of the mean.

inhibited $Ca_v1.2$ with IC_{50} values of $1.6 \pm 0.4\,\mu M$ and $2.8 \pm 0.9\,\mu M$, respectively. Against $Ca_v3.2$, **EM4** exhibited an IC_{50} of $0.6 \pm 0.3\,\mu M$, while **EM6** showed an IC_{50} of $1.4 \pm 0.2\,\mu M$.

Additionally, we conducted further experiments to investigate the state-dependent inhibition of $Ca_v1.2$ and $Ca_v3.2$ by **EM4**. Specifically, we evaluated how the blocking efficiency changes based on the membrane potential and the frequency of stimulation. For $Ca_v1.2$ and $Ca_v3.2$, under the standard testing condition, the cells were held at -90 mV and -120mV, respectively, and the testing frequency was 0.1 Hz. When the cells were held at more depolarized voltage (-60mV), the inhibition of currents increased significantly for both channel

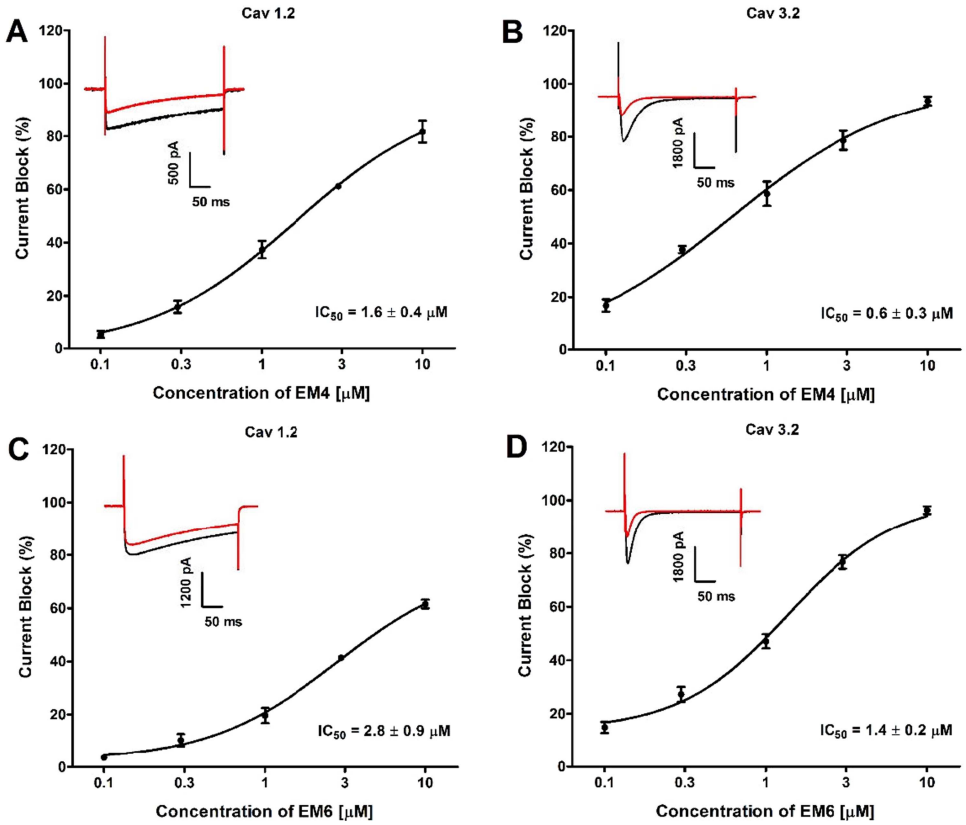

FIGURE 7 | Dose response curves for **EM4** (A, B) or **EM6** (C, D) inhibition of rat $Ca_v1.2$ or human $Ca_v3.2$ ($n = 3$ per dose). The inserts show representative currents in the absence and the presence of 1 μM tested compound.

subtypes, which indicated that the block was voltage dependent. Furthermore, when the testing frequency was increased from 0.1 Hz to 1 Hz, the degree of inhibition significantly increased for both channel isoforms, which demonstrated that the block was also frequency dependent (Figure 8). These data are overall consistent with the preferential block of inactivated channels.

3.4 | Enantiomeric Separation of EM4 and L-/T-Type Calcium Channel Blocking Activity of the Isomers

Chiral chromatographic separation of **EM1**-**EM15** have been previously reported (Sajeevan J et al. 2025). In this study, **EM4** was identified as one of the most potent inhibitors of both L- and T-type calcium channels in this series, according to the physiological data obtained. Hence, we sought to separate the stereoisomers of **EM4** to determine the inhibitory profile of each enantiomer. The enantioseparation of **EM4** using high-performance liquid chromatography (HPLC) resulted in two peaks with the following enantiomeric purities: Peak 1 (99.9%) and Peak 2 (98.2%) (Figure 9).

The structure of (***R***)-**EM4** was optimized (Figure 10) and the absolute configuration of the resolved enantiomers of **EM4** was determined using vibrational circular dichroism (VCD), which was (as is typical) performed in solution phase (Nafie et al. 2002; McGown et al. 2023). The infrared (IR) and VCD spectra of **EM4** peaks 1 and 2 were measured and the resulting experimental spectra were compared to DFT-calculated IR and

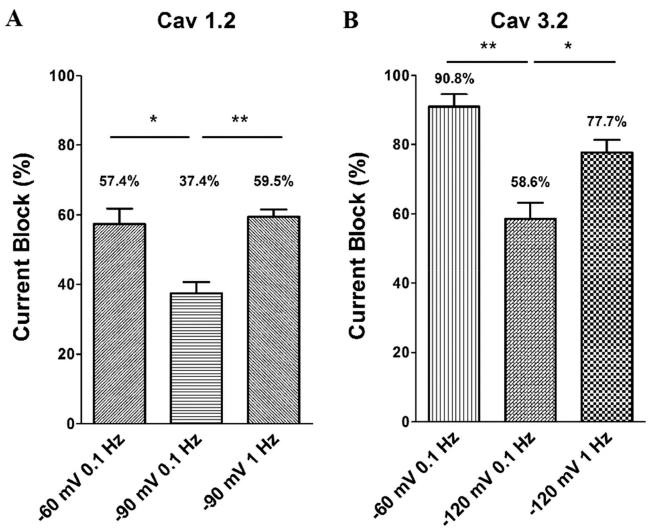

FIGURE 8 | Voltage dependence and frequency dependence of block of rat $Ca_v1.2$ (A) and human $Ca_v3.2$ (B) by 1 μM of **EM4** ($n = 3$). For $Ca_v1.2$ inhibition, $p = 0.02$ when comparing the holding potential of -90mV to -60mV, $p = 0.005$ when comparing the frequency of 0.1 Hz to 1 Hz (*t*-test). For $Ca_v3.2$ inhibition, $p = 0.005$ when comparing the holding potential of -120mV to -60mV, $p = 0.03$ when comparing the frequency of 0.1 Hz to 1 Hz (*t*-test). Asterisks denote statistical significance: $*p < 0.05$, $**p < 0.01$.

VCD spectra of the (*R*) enantiomer. **EM4** peak 1 was a very good match which allowed the assignment of (*R*) for peak 1 and (*S*) for peak 2 (Figure 11) (Debie et al. 2011; Polavarapu and Covington 2014).

Subsequently, the purified enantiomers were individually tested on $Ca_v1.2$ and $Ca_v3.2$. In both cases, the *R* enantiomer of **EM4**, referred to as Peak 1, presented better blocking capacity of L- and T-type calcium channels compared to the *S* isomer. (***R*)-EM4** inhibited $Ca_v1.2$ and $Ca_v3.2$ calcium currents with the inhibition values of 84.5% and 97.1%, respectively (Figure 12).

3.5 | Molecular Modeling Studies

In L-type channels, numerous DHPs have been shown to bind to a cavity close to the selectivity filter (Gao and Yan 2021; Zhao et al. 2019; Gao et al. 2023; Wei et al. 2024). This cavity is formed by segment 5 ($S5_{III}$), segment 6 ($S6_{III}$), the connecting segment 4-5 ($S4\text{-}5_{III}$) and the pore helix 1 ($P1_{III}$) of repeat III; and segment 6 ($S6_{IV}$) of repeat IV (Figure 13A) (Wu et al. 2015; Zhao et al. 2019; Gao et al. 2023; Wei et al. 2024). To investigate whether the EM compounds also target the DHP binding site and whether they can achieve a similar binding pose as other DHPs, molecular docking studies were performed for **EM4** and **EM6** in $Ca_v1.2$. Binding modes featuring a hydrogen bond to Ser1132, which is considered critical for blocking activity (Yamaguchi et al. 2000), were preferred over others, resulting in one final binding pose for ***(R)*-EM6** and ***(R)*-EM4** (Figures 13B and 14).

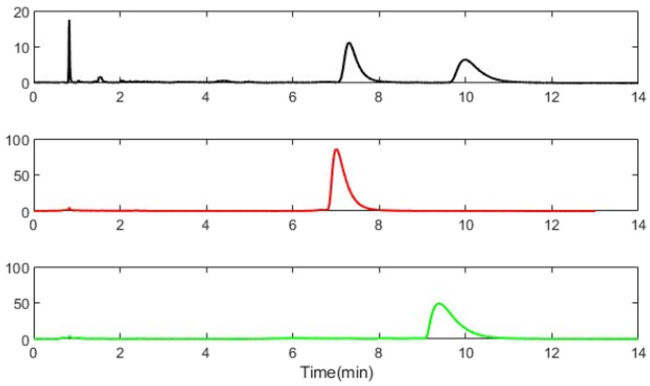

FIGURE 9 | Separation of the enantiomers of **EM4** using normal phase LC and chiral stationary phase. WhelkoShell 150 × 4.6 mm (i.d.) 2.7 μm SPP, 10/90 Ethanol/Hexanes, 2.50 mL/min, λ = 254 nm, 1 μL injection, (black) racemic mixture of **EM4**, (red) first peak of **EM4**, e.e. = 99.9%, (green) second peak of **EM4**, e.e. = 98.2%.

For the *S*-isomers, on the other hand, only binding modes with hydrophobic contacts were identified. These findings are consistent with the stereoselective activity testing, which showed that the *S*-isomer of **EM4** is less active than its *R*-isomer.

Therefore, we decided to conduct MD simulations only for the *R*-isomers in $Ca_v1.2$. ***(R)*-EM4** and ***(R)*-EM6** exhibit favorable shape similarity with amlodipine in $Ca_v1.2$, showing a similar binding mode to other DHPs. Both exhibit the critical hydrogen bond between the DHP nitrogen and Ser1132, while also forming hydrophobic contacts with their aromatic rings, halogens, the methyl group at C2; and the dimethyl moiety at C7 with their surrounding residues. In addition, the fluorine moiety of ***(R)*-EM4** acts as a hydrogen bond acceptor for Thr1056.

To investigate the binding modes of ***(R)*-EM4** and ***(R)*-EM6** in detail, dynophores were generated for ***(R)*-EM4** and ***(R)*-EM6** to reveal all protein-ligand interactions (Figure 15) (see Supporting Information S1: Table 1). Both ligands form the aforementioned hydrogen bonds between their DHP nitrogen and the Ser1132 hydroxyl oxygen and one hydrogen bond between their fluorine and the hydroxyl oxygen of Thr1056. Previous literature has shown that mutations of Ser1132 and Thr1056 lead to a decrease in blocking activity of DHPs (Mitterdorfer et al. 1996; Yamaguchi et al. 2000). Since our proposed binding mode is consistent with these findings, it suggests that both ligands may gain their blocking activity by binding to the DHP cavity.

For **(*R*)-EM4,** a hydrogen bond between the ester carbonyl oxygen and the hydroxyl oxygen of Thr1057 was observed. Compared to ***(R)*-EM4**, the carbonyl oxygen and amide nitrogen of ***(R)*-EM6** did not form any hydrogen bonds with their surrounding residues. We suspect that this is due to the missing rotatable bond between the amide nitrogen and aromatic ring, unlike ***(R)*-EM4**. The resulting rigid chain prevents the formation of any hydrogen bonds, which leads to a decrease in blocking activity of **(*R*)-EM6**. Our analysis reveals that a flexible side chain of the C3-ester moiety significantly improves $Ca_v1.2$ blocking activity of the ligand and potentially also improves binding affinity. Since ***(R)*-EM6** was analyzed to bind to the DHP cavity, we conclude that the DHP amides are suitable alternatives to develop novel calcium channel blockers.

For $Ca_v3.2$, an established concept for a DHP receptor is currently lacking. T-type selective antagonists such as ACT-709478 and TTA-A2 in $Ca_v3.2$ or Z944 in $Ca_v3.1$, have been shown to

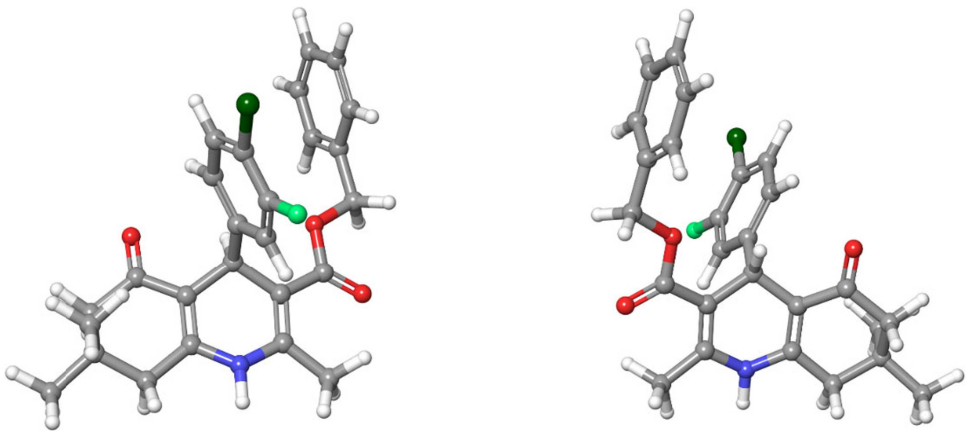

FIGURE 10 | The optimized structure of **(*R*)-EM4** presented in two different views.

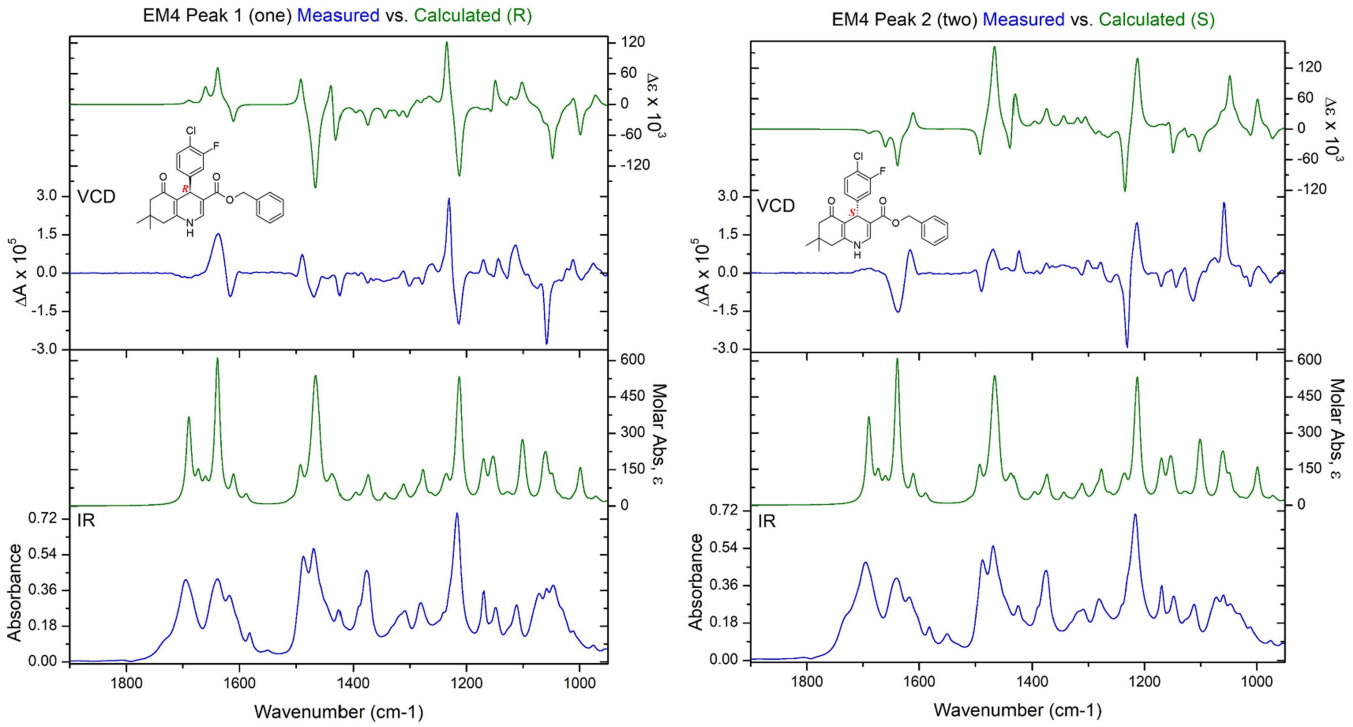

FIGURE 11 | A comparative analysis of experimental infrared spectra (IR) and vibrational circular dichroism (VCD) (represented by blue lines) of the **EM4** peaks with the DFT-calculated IR and VCD (depicted by green lines) for the respective enantiomers shows a close correlation. This indicates that the stereochemistry of Peak 1 is *R*, while Peak 2 corresponds to the *S* configuration.

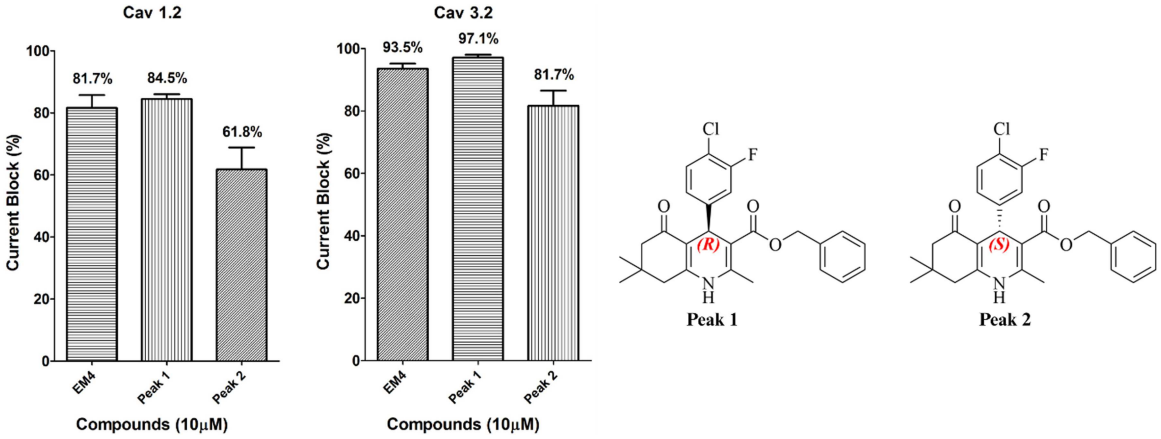

FIGURE 12 | Percentage of rCav1.2 and hCav3.2 current inhibition by **EM4** enantiomers (10 μM) and their chemical drawing indicating the configurations. $p = 0.03$ for the inhibition of $Ca_v1.2$ and $Ca_v3.2$ (one-way ANOVA, $n = 3$).

partially bind within the central cavity, obstructing ion flow and extend into the IV-I or II-III fenestration. The resolved structures to which these antagonists bind have been characterized as being in the inactivated, closed state, which is defined by four depolarized, or "up" voltage sensing domains and a closed intracellular gate. Pharmacologically, the binding mode of T-type selective antagonists has been described as a combination of pore blockage and allosteric antagonism, with a preference for inhibition of the inactivated state due to the fenestration blockage (Zhao et al. 2019; Huang et al. 2024; Tringham et al. 2012). Since EM compounds are non-selective T-type antagonists and block $Ca_v1.2$ and $Ca_v3.2$ with similar potency, we hypothesize that they bind to a non-selective binding site in $Ca_v3.2$, rather than the IV-I or II-III fenestration. In a recent study, the binding site of another non-selective series of compounds containing a DHP-based HHQ scaffold (**DA1**-**DA12**), was predicted to be located in the III-IV fenestration of $Ca_v3.2$ (Akman et al. 2022) analogous to the DHP binding site in $Ca_v1.2$.

Of particular interest is the potential binding mode of benidipine in $Ca_v3.2$, which is also classified as a non-selective calcium channel antagonist. It was analyzed to block over 50% of $Ca_v3.2$ inward current following comparable perfusion of 10 μM (Furukawa et al. 2009). Supported by docking experiments, Wei et al. hypothesized that non-selective DHP-based calcium channel antagonists such as benidipine bind to the III-IV fenestration site in T-type calcium channels (Wei et al. 2024).

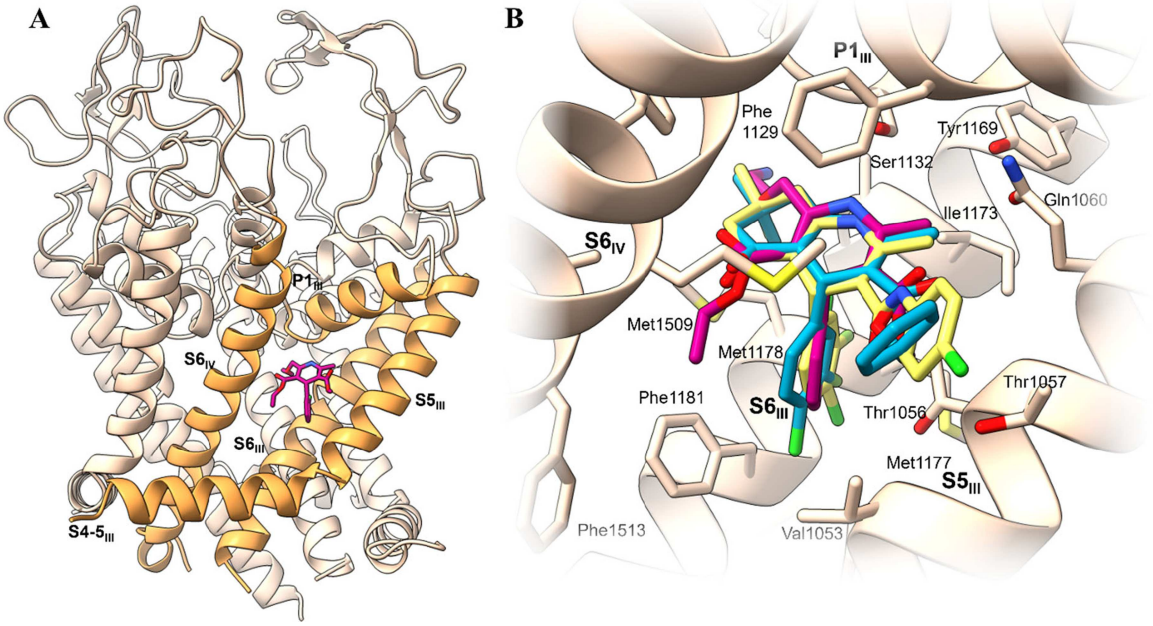

FIGURE 13 | Pore unit of $Ca_v1.2$ in complex with amlodipine (pink) (A), DHP binding site with amlodipine and docked ***(R)*-EM4** (blue) and ***(R)*-EM6** (yellow) (B).

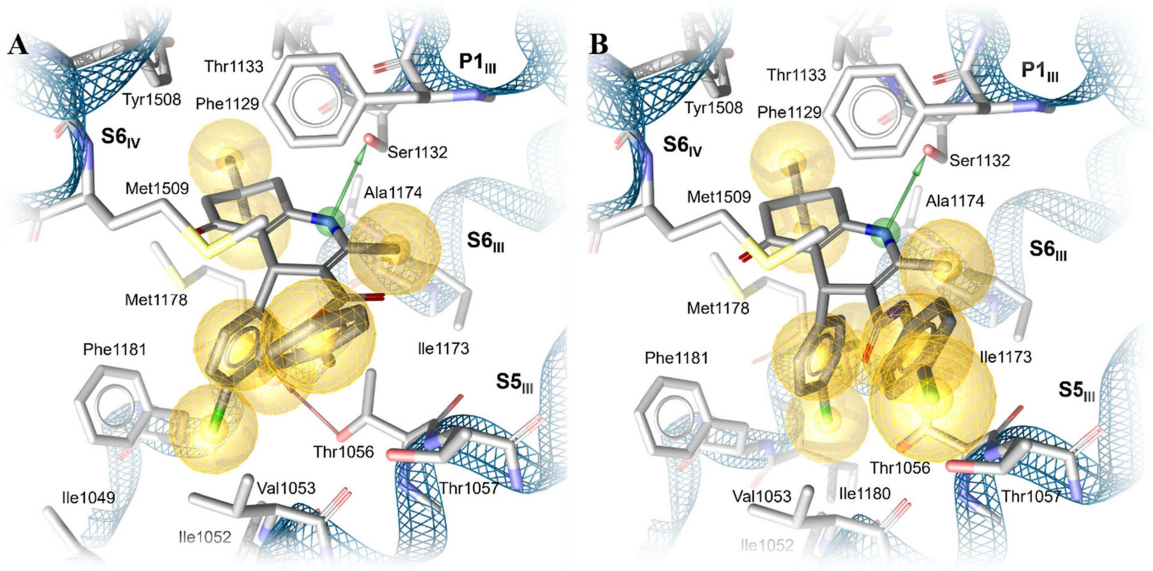

FIGURE 14 | Docking pose of ***(R)*-EM4** (A) and ***(R)*-EM6** (B) in $Ca_v1.2$. Yellow spheres depict hydrophobic contacts, red arrows and green arrows show hydrogen bond acceptors and hydrogen bond donors.

Therefore, we examined the III-IV fenestration site in the closed, inactivated $Ca_v3.2$ structure (PDB 9AYH) (Huang et al. 2024) for potential binding modes of ***(R)*-EM4** and ***(R)*-EM6** using molecular docking.

The docking results indicate that a hydrogen bond can be formed between the *N*-1 hydrogen of the HHQ scaffold and the backbone carbonyl oxygen of Ser1501, rather than the hydroxyl moiety of Ser1501 as previously reported. The difference is likely due to the presence of the bulky ester or amide side chain (Figure 16). Since interactions to the $P1_{III}$ loop have been reported to block ion flow by destabilizing the symmetry of the selectivity filter (Catterall et al. 2020), it is highly likely that an interaction with the backbone carbonyl has a similar effect.

For ***(R)*-EM4** and ***(R)*-EM6** two similar poses were identfied in which the carbonyl oxygen of the ester or the amide moiety formed a hydrogen bond with the hydroxyl moiety of Ser1501. In contrast to ***(R)*-EM6**, the longer *C*-3 ester side chain of ***(R)*-EM4** lacks interactions with the S5 segment of domain III. For the *N*-(4-chlorophenyl) side chain of the amide group in **(*R*)-EM6,** an additional halogen bond to Cys1438 was observed along with further lipophilic contacts to Phe1441 and Val1434. The distinct interaction pattern is consistent with the slightly higher blocking activity of **EM6** in $Ca_v3.2$. Furthermore, this interaction profile may explain the low blocking activity of **EM5,** in which the C3-side chain is *N*-phenylamide lacking the chlorine substituent, and consequently, the halogen bond.

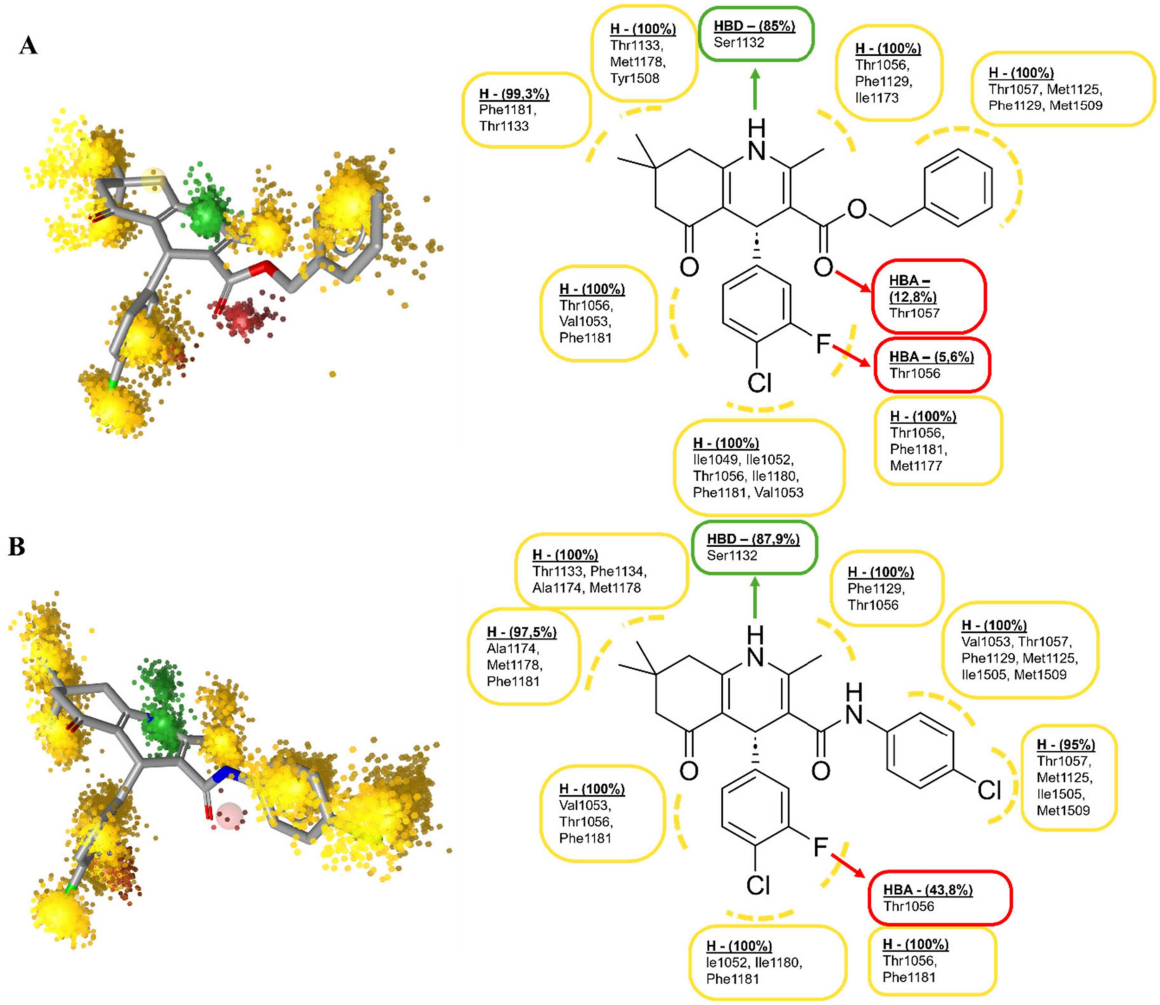

FIGURE 15 | Dynophores of ***(R)*-EM4** (A) and ***(R)*-EM6** (B) in $Ca_v1.2$ in two-dimensional and three-dimensional representation. Yellow dots depict hydrophobic contacts (H), while red and green dots represent hydrogen bond donors (HBD) and hydrogen bond acceptors (HBA). The percentage indicates the frequency of a specific interaction.

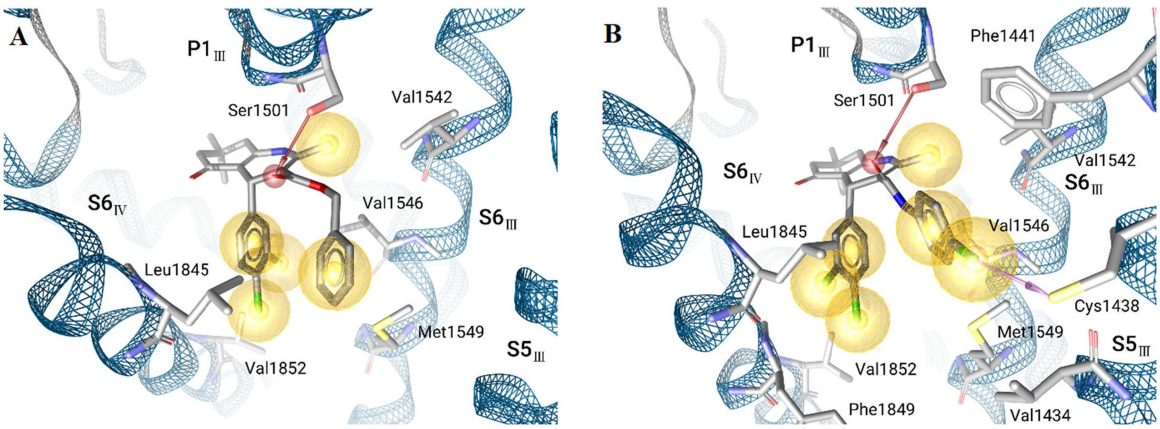

FIGURE 16 | Docking pose of ***(R)*-EM4** (A) and ***(R)*-EM6** (B) in $Ca_v3.2$. Yellow spheres depict hydrophobic contacts, red arrows show hydrogen bond acceptors and the purple arrow represents a halogen bond.

3.6 | Metabolic Stability Determination

Metabolic stability pertains to the susceptibility of a pharmaceutical compound to metabolic processes. A significant number of drugs administered orally undergo extensive clearance by the liver. Therefore, precise forecasting of hepatic metabolism and first-pass clearance is essential during the initial phases of drug discovery and development (Masimirembwa et al. 2003; Gajula et al. 2021). Our goal in this study was to investigate the metabolic stability of our compounds and assess the impact of ester and amide functionalities on this stability. We chose

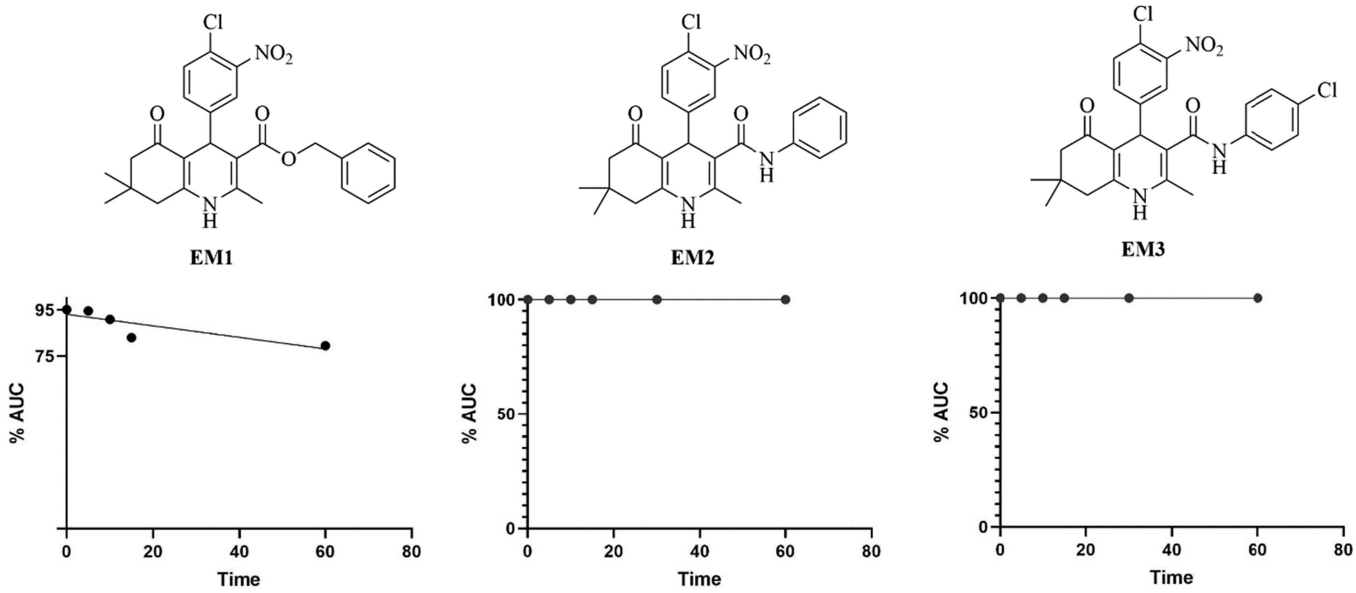

FIGURE 17 | Metabolic stability results of **EM1**-**EM3** with their chemical structures.

compounds **EM1**-**EM3,** which have the same aryl group and all blocked both types of calcium channels. According to the data obtained, all tested compounds were found to be stable in microsomal environment. **EM1** that possesses ester functionality showed less stability compared to amide counterparts. Nevertheless, the $t_{1/2}$ of **EM1** was recorded as > 60 min for a 60 min procedure assay. On the other hand, for **EM2** and **EM3**, the presence of the amide moiety provided metabolic stability (Figure 17). Our findings support the in vivo stability of amide functional group and highlights its significance in improving metabolic stability (Kumari et al. 2020).

3.7 | Structure-Activity Relationship

To explore the structure-activity relationships of HHQs with calcium channel blocking activity, we correlated the chemical structures of **EM1**-**EM15** with the physiological data obtained, as well as the results from molecular modeling and metabolic stability studies. The key conclusions from our findings are summarized as follows:

- The primary chemical difference between the compounds lies in the type of carbonyl group (ester or amide) they contain. According to patch-clamp assays, ester derivatives were more effective calcium channel blockers; however, amide counterparts demonstrated a significant degree of blocking on calcium currents carried by both $Ca_v1.2$ and $Ca_v3.2$. The amide side chain of our compounds was rigid, which resulted in the formation of no hydrogen bonds between the carbonyl oxygen or amide nitrogen and the calcium channel, as observed in molecular modeling studies within $Ca_v1.2$. Therefore, designing amide-carrying HHQs by introducing flexible amide moieties is likely to result in more effective calcium channel blockers.
- The incorporation of a chlorine atom at the *para* position of the phenyl ring in amide-functionality of HHQs led to a notable increase in the activity of these derivatives. This increase in activity can be attributed to the enhanced hydrophobic interactions or the halogen bonding with the calcium channel facilitated by the chlorine substitution, according to molecular docking studies.
- Amide-possessing HHQs were found to be metabolically more stable in comparison with their ester counterparts. This finding highlights the importance of designing more amide-based HHQs as potential calcium channel inhibitors for the treatment of various cardiovascular and neurological disorders.
- At the C-4 position of the HHQ scaffold, the phenyl ring has different groups attached to it at the same locations. As a result, we can directly link the type of substituent to the calcium channel blocking ability of the compounds. Particularly, the substitution of methoxy groups onto the C-4 phenyl ring (**EM10**-**EM13**)was not preferential for calcium channel blocking activity. Except for **EM4**, **EM1**-**EM9** all showed effective inhibition against $Ca_v1.2$ and $Ca_v3.2$. According to molecular modeling studies, these derivatives have a chlorine atom at the *para* position of the phenyl ring, which forms hydrophobic contacts with $Ca_v1.2$ and $Ca_v3.2$. At the *meta* position, hydrogen bond acceptors such as NO_2, CF_3, and F were favorable substituents for interacting with the channel. Among them, fluorine, in addition to hydrophobic interactions, can also participate in hydrogen bonding as a hydrogen bond acceptor, as observed in $Ca_v1.2$. Changing the aromatic substitution pattern in **EM10**-**EM15** reduced the inhibitory activity against $Ca_v1.2$. The 1,3-benzodioxole ring at C-4 of HHQs (**EM13** and **EM15**) allowed us to identify selective blockers of $Ca_v3.2$ over $Ca_v1.2$. This result aligned with our previous findings (Akman et al. 2022; Koçak Aslan et al. 2024).

4 | Conclusions

In order to gain a deeper understanding of the structure-activity relationships of DHP-based calcium channel blockers, we synthesized fifteen compounds possessing HHQ scaffold with either an ester or an amide moiety. The target molecules,

obtained using a modified Hantzsch method, were evaluated for their effects on L-($Ca_v1.2$) and T-($Ca_v3.2$)-type calcium channels through the application of the whole-cell patch clamp technique. According to the inhibition values, while the amide derivatives exhibited slightly lower activity compared to their ester counterparts, they still inhibited calcium currents through L- and T-type channels to a considerable degree. The block of both calcium channel subtypes by **EM4** was demonstrated to be voltage- and frequency-dependent. The enantiomers of **EM4** were separated using HPLC on a chiral stationary phase. Subsequent testing on the $Ca_v1.2$ and $Ca_v3.2$ channels revealed that the *R*-isomer demonstrated a greater efficacy in inhibiting both types of calcium channels. Molecular docking and dynophore analysis provided mechanistic insight into the observed physiological profiles. In $Ca_v1.2$, both (***R***)-**EM4** and (***R***)-**EM6** were shown to bind within the well studied DHP binding pocket, adopting binding modes comparable to clinically used DHPs and forming a conserved hydrogen bond with Ser1132 that is critical for channel blockade. However, our analysis revealed that the ester derivative (***R***)-**EM4** exhibits greater conformational stability than the amide derivative (***R***)-**EM6**, which was attributed to increased flexibility of the ester side chain and its ability to better accommodate stabilizing hydrogen bonds between the carbonyl oxygen and Thr1057. For $Ca_v3.2$, docking studies suggested that both compounds interact with the III–IV fenestration, a proposed non-selective DHP binding site in T-type calcium channels. Notably, the amide derivative (***R***)-**EM6** engages in additional lipophilic contacts and forms a stabilizing halogen bond that are absent in the ester analogue (***R***)-**EM4**, providing a structural rationale for the high blocking activity of **EM6** at $Ca_v3.2$. Besides this, even being slightly less effective against calcium channels, amide derivatives were demonstrated to be metabolically more stable than their ester counterparts. Altogether, our data demonstrates for the first time that amide-bearing HHQs hold significant promise for the design of further calcium channel blockers as potential therapeutics against cardiovascular and pain disorders.

Acknowledgments

The authors acknowledge the Scientific and Technological Research Application and Research Center, Sinop University, Turkey, for the use of the Bruker D8 QUEST diffractometer. A.K. gratefully acknowledges the financial support provided by The Scientific and Technological Research Council of Türkiye (TÜBİTAK) through the 2211-A National PhD Scholarship Program. M.G.G, E.K.A., and A.K. would like to thank Hacettepe University Scientific Research Projects Coordination Unit for the financial support provided through Project THD-2024-21388. G.W.Z. acknowledges the financial support of Natural Sciences and Engineering Research Council of Canada. We gratefully acknowledge the separation work by Siddharth Jaya Sajeevan J and Reza Salehi of the University of Texas at Arlington.

Ethics Statement

The rat livers were donated by Acibadem University, Animal Laboratory Centre from the Project by Dr. Mehmet Emin Aksoy; laparoscopic and robotic surgery, with the 2021-01 ethical approval number. At the end of the training, liver tissue was obtained from the euthanized rat.

Conflicts of Interest

The authors declare no conflicts of interest.

Data Availability Statement

The data that support the findings of this study are available from the corresponding author upon reasonable request.

References

Akman, D., K. Denzinger, S. Huang, et al. 2022. "Focusing on C-4 Position of Hantzsch 1,4-Dihydropyridines: Molecular Modifications, Enantioseparation, and Binding Mechanism to L- and T-Type Calcium Channels." *European Journal of Medicinal Chemistry* 244: 114787.

Armstrong, D. W., J. Yu, H. D. Cole, S. A. McFarland, and J. Nafie. 2021. "Chiral Resolution and Absolute Configuration Determination of New Metal-Based Photodynamic Therapy Antitumor Agents." *Journal of Pharmaceutical and Biomedical Analysis* 204: 114233.

Aygün Cevher, H., D. Schaller, M. A. Gandini, et al. 2019. "Discovery of Michael Acceptor Containing 1,4-Dihydropyridines as First Covalent Inhibitors of L-/T-Type Calcium Channels." *Bioorganic Chemistry* 91: 103187.

Bain, A. 2019. "Use of Calcium Channel Blockers in Cardiovascular Disease." *British Journal of Cardiac Nursing* 14, no. 2: 64–70.

Bandyopadhyay, D., T. Salazar, and A. Gonzalez. 2017. "Dihydropyridines as Calcium Channel Blockers: An Overview." *Journal of Analytical & Pharmaceutical Research* 5, no. 4: 00148.

Bkaily, G., and D. Jacques. 2023. "Calcium Homeostasis, Transporters, and Blockers in Health and Diseases of the Cardiovascular System." *International Journal of Molecular Sciences* 24, no. 10: 8803.

Bladen, C., V. M. Gadotti, M. G. Gündüz, et al. 2015. "1,4-Dihydropyridine Derivatives With T-Type Calcium Channel Blocking Activity Attenuate Inflammatory and Neuropathic Pain." *Pflügers Archiv - European Journal of Physiology* 467, no. 6: 1237–1247.

Bladen, C., M. G. Gündüz, R. Şimşek, C. Şafak, and G. W. Zamponi. 2014. "Synthesis and Evaluation of 1,4-Dihydropyridine Derivatives With Calcium Channel Blocking Activity." *Pflügers Archiv - European Journal of Physiology* 466, no. 7: 1355–1363.

Bruker AXS Inc. Madison Wisconsin USA. 2012. APEX3.

Cai, S., K. Gomez, A. Moutal, and R. Khanna. 2021. "Targeting T-Type/CaV3.2 Channels for Chronic Pain." *Translational Research* 234: 20–30.

Catterall, W. A. 2023. "Voltage Gated Sodium and Calcium Channels: Discovery, Structure, Function, and Pharmacology." *Channels* 17, no. 1: 2281714.

Catterall, W. A., M. J. Lenaeus, and T. M. Gamal El-Din. 2020. "Structure and Pharmacology of Voltage-Gated Sodium and Calcium Channels." *Annual Review of Pharmacology and Toxicology* 60: 133–154.

Debie, E., E. De Gussem, R. K. Dukor, W. Herrebout, L. A. Nafie, and P. Bultinck. 2011. "A Confidence Level Algorithm for the Determination of Absolute Configuration Using Vibrational Circular Dichroism or Raman Optical Activity." *Chemphyschem* 12, no. 8: 1542–1549.

Farrugia, L. J. 2012. "WinGX and ORTEP for Windows: An Update." *Journal of Applied Crystallography* 45, no. 4: 849–854.

Freedman, T. B., X. Cao, R. K. Dukor, and L. A. Nafie. 2003. "Absolute Configuration Determination of Chiral Molecules in the Solution State Using Vibrational Circular Dichroism." *Chirality* 15, no. 9: 743–758.

Furukawa, T., T. Nukada, Y. Namiki, et al. 2009. "Five Different Profiles of Dihydropyridines in Blocking T-Type Ca2+ Channel Subtypes (Cav3.1 (A1G), Cav3.2 (A1H), and Cav3.3 (A1I)) Expressed in Xenopus Oocytes." *European Journal of Pharmacology* 613, no. 1–3: 100–107.

Gajula, S. N. R., N. Nadimpalli, and R. Sonti. 2021. "Drug Metabolic Stability in Early Drug Discovery to Develop Potential Lead Compounds." *Drug Metabolism Reviews* 53, no. 3: 459–477.

Gao, S., and N. Yan. 2021. "Structural Basis of the Modulation of the Voltage-Gated Calcium Ion Channel Cav1.1 by Dihydropyridine

Compounds**." *Angewandte Chemie International Edition* 60, no. 6: 3131–3137.

Gao, S., X. Yao, J. Chen, et al. 2023. "Structural Basis for Human Cav1.2 Inhibition by Multiple Drugs and the Neurotoxin Calciseptine." *Cell* 186, no. 24: 5363–5374.e16.

Glaser, T., V. F. Arnaud Sampaio, C. Lameu, and H. Ulrich. 2019. "Calcium Signalling: A Common Target in Neurological Disorders and Neurogenesis." *Seminars in Cell & Developmental Biology* 95: 25–33.

Halgren, T. A. 1996. "Merck Molecular Force Field. I. Basis, Form, Scope, Parameterization, and Performance of MMFF94." *Journal of Computational Chemistry* 17, no. 5–6: 490–519.

Harding, E. K., and G. W. Zamponi. 2022. "Central and Peripheral Contributions of T-Type Calcium Channels in Pain." *Molecular Brain* 15, no. 1: 39.

Hofmann, F., V. Flockerzi, S. Kahl, and J. W. Wegener. 2014. "L-Type CaV1.2 Calcium Channels: From In Vitro Findings to In Vivo Function." *Physiological Reviews* 94, no. 1: 303–326.

Huang, J., X. Fan, X. Jin, et al. 2024. "Structural Basis for Human Cav3.2 Inhibition by Selective Antagonists." *Cell Research* 34, no. 6: 440–450.

Jones, G., P. Willett, R. C. Glen, A. R. Leach, and R. Taylor. 1997. "Development and Validation of a Genetic Algorithm for Flexible Docking." *Journal of Molecular Biology* 267, no. 3: 727–748.

Jones, K. E., S. L. Hayden, H. R. Meyer, et al. 2024. "The Evolving Role of Calcium Channel Blockers in Hypertension Management: Pharmacological and Clinical Considerations." *Current Issues in Molecular Biology* 46, no. 7: 6315–6327.

Jorgensen, W. L., D. S. Maxwell, and J. Tirado-Rives. 1996. "Development and Testing of the OPLS All-Atom Force Field on Conformational Energetics and Properties of Organic Liquids." *Journal of the American Chemical Society* 118, no. 45: 11225–11236.

Koçak Aslan, E., K. Lam, C. Dengiz, et al. 2024. "Synthesis, Molecular Modeling, DFT Studies, and EPR Analysis of 1,4-Dihydropyridines as Potential Calcium Channel Blockers." *Journal of Molecular Structure* 1307: 137983.

Kumari, S., A. V. Carmona, A. K. Tiwari, and P. C. Trippier. 2020. "Amide Bond Bioisosteres: Strategies, Synthesis, and Successes." *Journal of Medicinal Chemistry* 63, no. 21: 12290–12358.

MacRae, C. F., I. Sovago, S. J. Cottrell, et al. 2020. "Mercury 4.0: From Visualization to Analysis, Design and Prediction." *Journal of Applied Crystallography* 53, no. 1: 226–235.

Masimirembwa, C. M., U. Bredberg, and T. B. Andersson. 2003. "Metabolic Stability for Drug Discovery and Development: Pharmacokinetic and Biochemical Challenges." *Clinical Pharmacokinetics* 42, no. 6: 515–528.

McGown, A., J. Nafie, M. Otayfah, et al. 2023. "Chirality: A Key Parameter in Chemical Probes." *RSC Chemical Biology* 4, no. 10: 716–721.

Meanwell, N. A. 2023. "Applications of Bioisosteres in the Design of Biologically Active Compounds." *Journal of Agricultural and Food Chemistry* 71, no. 47: 18087–18122.

Mitterdorfer, J., Z. Wang, M. J. Sinnegger, et al. 1996. "Two Amino Acid Residues in the IIIS5 Segment of L-Type Calcium Channels Differentially Contribute to 1,4-Dihydropyridine Sensitivity." *Journal of Biological Chemistry* 271, no. 48: 30330–30335.

Nafie, L. A., R. K. Dukor, and T. B. Freedman. 2002. "Vibrational Circular Dichroism." In *Handbook of Vibrational Spectroscopy*, 731–744. Wiley.

Nahler, G. 2009. "Anatomical Therapeutic Chemical Classification System." In *Dictionary of Pharmaceutical Medicine*. Springer Vienna.

Pelin COŞKUN, G., E. G. Algin, J. C. Karakoç, B. T. Erbul, and M. Ülgen. 2023. "Formation of N-Oxide Metabolites From Isoniazid Hydrazones of Substituted Benzaldehydes by Hepatic Washed Pig Microsomal Preparations." *Journal of Research in Pharmacy* 27, no. 1: 241–250.

Polavarapu, P. L., and C. L. Covington. 2014. "Comparison of Experimental and Calculated Chiroptical Spectra for Chiral Molecular Structure Determination." *Chirality* 26, no. 9: 539–552.

Saini, K. K., R. Rani, I. Muskan, N. Khanna, B. Mehta, and R. Kumar. 2023. "An Overview of Recent Advances in Hantzsch's Multicomponent Synthesis of 1,4- Dihydropyridines: A Class of Prominent Calcium Channel Blockers." *Current Organic Chemistry* 27, no. 2: 119–129.

Sajeevan J, S. J., R. Salehi, R. J. Burk, et al. 2025. "Chiral Chromatographic Separation of Fifteen New Hexahydroquinoline Derivatives." *Chirality* 37, no. 5: e70033.

Schaller, D., M. G. Gündüz, F. X. Zhang, G. W. Zamponi, and G. Wolber. 2018. "Binding Mechanism Investigations Guiding the Synthesis of Novel Condensed 1,4-Dihydropyridine Derivatives With L-/T-Type Calcium Channel Blocking Activity." *European Journal of Medicinal Chemistry* 155: 1–12.

Schaller, D., D. Šribar, T. Noonan, et al. 2020. "Next Generation 3D Pharmacophore Modeling." *WIREs Computational Molecular Science* 10, no. 4: 1–20.

Sheldrick, G. M. 2008. "A Short History of SHELX." *Acta Crystallographica. Section A: Foundations of Crystallography* 64, no. 1: 112–122.

Sheldrick, G. M. 2015. "Crystal Structure Refinement With SHELXL." *Acta Crystallographica, Section C: Structural Chemistry* 71, no. 1: 3–8.

Tringham, E., K. L. Powell, S. M. Cain, et al. 2012. "T-Type Calcium Channel Blockers That Attenuate Thalamic Burst Firing and Suppress Absence Seizures." *Science Translational Medicine* 4, no. 121: 121ra19.

Wei, Y., Z. Yu, L. Wang, et al. 2024. "Structural Bases of Inhibitory Mechanism of CaV1.2 Channel Inhibitors." *Nature Communications* 15, no. 1: 2772.

Weiss, N., and G. W. Zamponi. 2019. "T-Type Calcium Channels: From Molecule to Therapeutic Opportunities." *International Journal of Biochemistry & Cell Biology* 108: 34–39.

Weiss, N., and G. W. Zamponi. 2023. "The T-Type Calcium Channelosome." *Pflügers Archiv - European Journal of Physiology* 476, no. 2: 163–177.

Wolber, G., A. A. Dornhofer, and T. Langer. 2006. "Efficient Overlay of Small Organic Molecules Using 3D Pharmacophores." *Journal of Computer-Aided Molecular Design* 20, no. 12: 773–788.

Wolber, G., and T. Langer. 2005. "LigandScout: 3-D Pharmacophores Derived From Protein-Bound Ligands and Their Use as Virtual Screening Filters." *Journal of Chemical Information and Modeling* 45, no. 1: 160–169.

Wu, J., Z. Yan, Z. Li, et al. 2015. "Structure of the Voltage-Gated Calcium Channel Cav1.1 Complex." *Science* 350, no. 6267: aad2395.

Yamaguchi, S., Y. Okamura, T. Nagao, and S. Adachi-Akahane. 2000. "Serine Residue in the IIIS5-S6 Linker of the L-Type Ca2+ Channel A1C Subunit Is the Critical Determinant of the Action of Dihydropyridine Ca2+Channel Agonists." *Journal of Biological Chemistry* 275, no. 52: 41504–41511.

Zhao, Y., G. Huang, J. Wu, et al. 2019. "Molecular Basis for Ligand Modulation of a Mammalian Voltage-Gated Ca2+ Channel." *Cell* 177, no. 6: 1495–1506.e12.

Zhao, Y., G. Huang, Q. Wu, et al. 2019. "Cryo-EM Structures of Apo and Antagonist-Bound Human Cav3.1." *Nature* 576, no. 7787: 492–497.

Supporting Information

Additional supporting information can be found online in the Supporting Information section.
^{1}H NMR, ^{13}C NMR, and HRMS spectra of the synthesized compounds, along with detailed methods of experimental and computational studies.